Acc. Chem. Res. **1998,** *31,* 219−227

New Organic Materials Suitable for Use in Chemical Sensor Arrays

RICHARD M. CROOKS*,†

Department of Chemistry, Texas A&M University, P.O. Box 300012, College Station, Texas 77842

ANTONIO J. RICCO*,‡

Microsensor R&D Department, Sandia National Laboratories, Albuquerque, New Mexico 87185-1425

Received August 20, 1997

Introduction

In an accompanying article in this issue,[1] Ricco et al. discuss some of the advantages of using chemical sensor arrays for many analytical and detection applications. Array-based sensing involves four distinct conceptual steps: development of suitable chemically sensitive interfacial materials, integration of these materials onto sensor transducers, development of pattern-recognition algorithms,[2] and system integration and packaging. In this Account we address the first, and arguably the least technologically developed, of these four steps.

There is no single best approach for developing chemically selective interfaces. The appropriateness of the materials depends entirely on the application and the operating environment. Nevertheless, there are a number of important factors to consider in developing optimal interfacial materials for chemical sensor arrays: the thickness and structure of the material, the uniqueness of its response to analytes or classes of analytes, ease of synthesis, cost, and durability to name a few. The majority of commercially available sensors rely on inorganic materials primarily because of their durability and suitability for operation at elevated temperatures. Inorganic materials will certainly be an important part of next-generation array sensors, but organic materials will play an expanding role because of the vast menu of physical and chemical properties they provide. In particular, organic materials lend themselves to synthetic flexibility, which implies that they can be tailored to exhibit a high level of *chemical independence* and structural order. The important concept of chemical independence is discussed in another article in this issue.[1] Briefly, however, a material displays chemical independence when it responds to an analyte or class of analytes in a manner distinct from other materials used in the array. That is, a chemically independent material provides a response that *cannot* be expressed as an analyte-invariant combination of the responses of the other materials used in the array.[1]

The objectives, then, in designing organic materials for use in chemical sensor arrays are as follows. First, the materials should be synthetically flexible so that they can be tailored to be chemically independent. Second, they should be cheap, durable, and easy to immobilize on the transducer surface. Third, they should be configured on the surface such that they respond sufficiently quickly to the presence of an analyte to meet the needs of the application. Although this often implies the use of thin films such as monolayers, the sensor may need to function over a large dynamic range of analyte concentrations prior to receptor saturation, which implies thicker polymeric materials.

In this Account, we describe three recently developed types of materials that approach the aforementioned objectives: self-assembled monolayers (SAMs), self-assembled bilayers, and dendrimer monolayers. The focus of the work described here is on the synthesis, characterization, and surface immobilization of these materials, but we also report the results of some preliminary experiments aimed specifically at chemical sensing applications.

Monolayers

Monolayer self-assembly chemistry is useful for constructing functional organic surfaces.[3−5] For example, monolayers of *n*-alkanethiols spontaneously adsorb to Au from liquid and vapor phases.[4−8] The resulting monolayer assumes a $(\sqrt{3} \times \sqrt{3})$R30° overlayer structure on Au(111) (Scheme 1). Analyses indicate that this class of self-assembled monolayer (SAM) is composed of hydrocarbon chains tilted 30−40° from the surface normal; SAMs prepared from shorter chains are more disordered than those formed from longer-chain molecules, and defects are thought to result primarily from missing molecules and gauche conformations within the energetically more favorable all-trans, extended SAM structure. SAMs are fairly robust in gas-phase ambients at temperatures below 100 °C.[4−8]

SAMs typically, but not always, derive their chemical selectivity from the outermost few angstroms of the film,

Richard M. Crooks received his Bachelor of Science degree in chemistry from the University of Illinois (Urbana, IL) and his doctoral degree in electrochemistry from the University of Texas (Austin, TX) in 1987. He is currently Professor of Chemistry at Texas A&M University (College Station, TX). His research interests include chemical sensors and interfacial design, electrocatalysis, corrosion and corrosion inhibition, physical electrochemistry, and the molecular basis of adhesion and adhesive interactions.

Antonio J. Ricco was born in Oakland, CA in 1958. He received a B.S. in chemistry (magna cum laude) from the University of California, Berkeley, in 1980 and a Ph.D. in inorganic chemistry from the Massachusetts Institute of Technology in 1984. He joined Sandia National Laboratories' Microsensor Research Division in 1984, where his research currently involves chemical sensor arrays based on acoustic wave, optical, electrochemical, and various microelectronic platforms. He focuses on new ways to utilize chemical and physical effects together with new materials in combination with microelectronic technology and pattern recognition to develop novel chemical sensors with enhanced capabilities.

* To whom correspondence should be addressed.
† E-mail: crooks@chemvx.tamu.edu. Phone: (409) 845-5629. Fax: (409) 845-1399.
‡ E-mail: ajricco@sandia.gov. Phone: (505) 844-1405. Fax: (505) 844-1198.

S0001-4842(97)00246-X CCC: $15.00
Published on Web 04/17/1998

Scheme 1

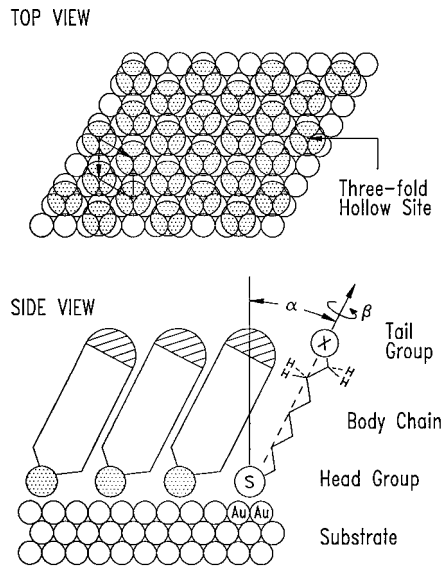

Scheme 2

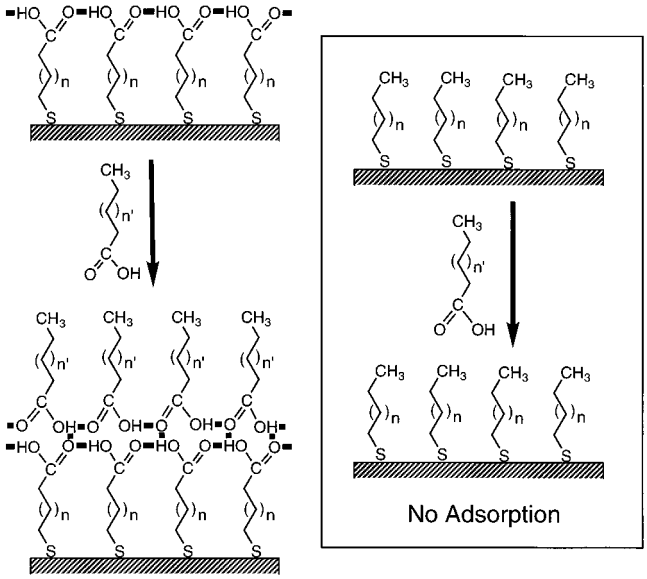

which generally corresponds to the terminal functional groups.[7,9,10] Terminal groups, and thus chemical sensitivity, can be manipulated either prior to surface immobilization [7,9,10] or by chemical reaction following self-assembly of a suitable intermediate attachment layer.[11−14] SAM interfaces have the advantage of being easily and reproducibly synthesized, and, because analytes do not have to permeate through a diffusion barrier as they do for thicker polymer films, the sorption rate is typically fast. There are two principal disadvantages to the use of monolayer films, however. First, because chemical selectivity depends only on the termial group, the degree of chemical selectivity that can be engineered into a simple SAM may not be as great as in thicker or more complex materials. Second, the total number of receptors incorporated into the film, and thus the dynamic range and sensitivity of the sensor, is limited by the surface area of the substrate.

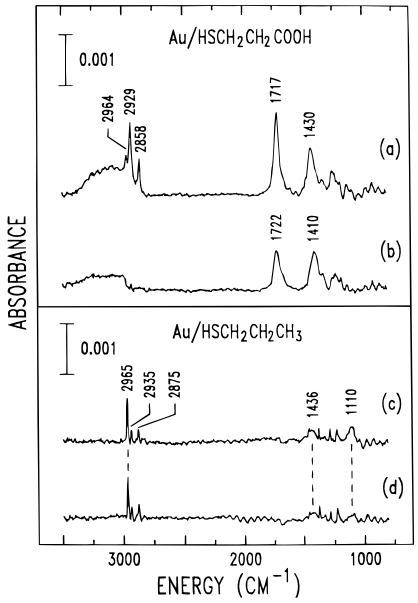

FIGURE 1. FTIR-ERS spectra of a Au/HS$(CH_2)_2$COOH surface before (b) and after (a) exposure to vapor-phase $CH_3(CH_2)_{12}$COOH. FTIR-ERS spectra of a Au/HS$(CH_2)_2CH_3$ surface before (d) and after (c) exposure to vapor-phase $CH_3(CH_2)_{12}$COOH. Only the acid-terminated SAM is receptive to binding of $CH_3(CH_2)_{12}$COOH, as indicated by the doubling of the carbonyl band at 1717 cm^{-1} and the increase of the methylene and methyl modes at high energy in part (a).

SAMs prepared from carboxylic acid-functionalized organomercaptans provide a very simple illustration of how monolayers can be tailored to achieve chemical selectivity. The terminal acid groups interact with acidic or basic vapor-phase molecules by hydrogen bonding or by proton-transfer interactions, respectively.[15,16] Hydrogen-bonding systems are typified by the interactions of *n*-alkanoic acids ($CH_3(CH_2)_n$COOH, $n = 0-14$) with Au surfaces modified with 3-mercaptopropionic acid (Au/HS-$(CH_2)_2$COOH) (Scheme 2).

Figure 1 shows FTIR-ERS data for Au/HS$(CH_2)_2$COOH and Au/HS$(CH_2)_2CH_3$ surfaces after and before exposure to a saturated vapor of myristic acid, $CH_3(CH_2)_{12}$COOH. Prior to $CH_3(CH_2)_{12}$COOH dosing, the Au/HS$(CH_2)_2$COOH spectrum, Figure 1b, reveals bands due to the acid C═O stretch and the enhanced a-CH_2 scissors mode at 1722 and 1410 cm^{-1}, respectively. After dosing, the presence of a second surface-confined $CH_3(CH_2)_{12}$COOH layer (Scheme 2) is confirmed by the appearance of the methyl C−H stretching vibration at 2964 cm^{-1}, the increased intensity of the methylene C−H stretching vibrations at 2929 and 2858 cm^{-1}, and the doubling of the intensity of the C═O stretching vibration at 1717 cm^{-1} (Figure 1a). The positions of the carbonyl bands in these two spectra indicate that the myristic acid is bound to the SAM by strong hydrogen bonds as indicated in Scheme 2.

To demonstrate that the acid-terminated SAM specifically selects for other acids, we also exposed a methylated surface to vapor-phase *n*-alkanoic acids as shown on the right side of Scheme 2. The FTIR-ERS spectrum of a surface-confined monolayer of HS$(CH_2)_2CH_3$ is shown in Figure 1d. The bands at high energy result from C−H stretching modes, while other peaks attributable to hy-

Scheme 3

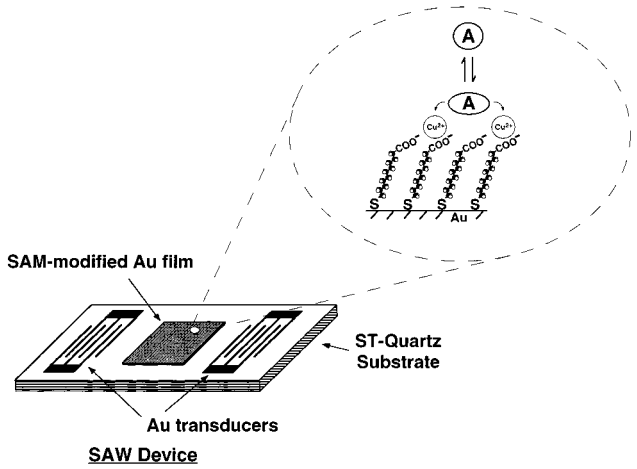

drocarbon backbone modes are present at lower frequencies. The FTIR-ERS spectrum of the methyl surface after exposure to $CH_3(CH_2)_{12}COOH$, Figure 1c, is identical with the surface before acid dosing. This result clearly shows that only the acid surface is selective for acid-functionalized analytes and thus that these two sensor surfaces respond very differently to the chemical class of acidic materials.

Simple Bilayers

Self-assembled films of complex molecules and molecular assemblies are generally more difficult to prepare than simple alkyl-based materials. However, stepwise self-assembly of simple materials can lead to enhanced versatility via more complex systems. For example, a simple organomercaptan SAM can act as a coupling layer for a more specific receptor. In the case of the just-described acid-terminated SAM, the material's scope and versatility are readily expanded by a simple chemical trick. The coating design discussed in this section takes advantage of the affinity of the deprotonated form of the acid-terminal groups of mercaptoundecanoic acid (MUA) for many different metal ions, including Ag^+, Cu^{2+}, Ni^{2+}, Zn^{2+}, Fe^{3+}, La^{3+}, and Zr^{4+}, to yield a host of different chemically selective metal-carboxylate interfaces. Some of these interact strongly with organophosphonates such as the nerve-agent simulant diisopropyl methylphosphonate (DIMP) and, presumably, the Type G nerve agents to which it is related. We chose to examine the Au/MUA-Cu^{2+} interface in detail because Cu^{2+} is a hydrolysis catalyst for certain nerve agents,[17] and we reasoned that good catalytic materials would also perform well as sensor interfaces since both involve selective and reversible interactions with analytes.

The metal-ion/acid bilayers are very easy to prepare. The MUA monolayer is assembled by soaking a Au substrate in a dilute ethanolic solution of MUA for a few hours (or longer), then dipping it into a dilute ethanolic solution of the metal ion for a few minutes, rinsing with ethanol, and drying. The formation of a MUA-Cu^{2+}-terminated monolayer (inset of Scheme 3) is easily confirmed by X-ray photoelectron spectroscopy (XPS)

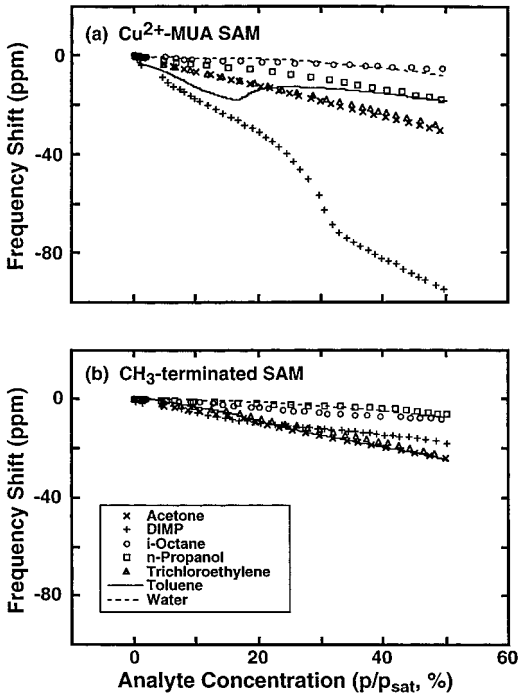

FIGURE 2. Adsorption isotherms for a SAW device coated with either a (a) MUA-Cu^{2+}- or (b) CH_3-terminated SAM, exposed to six different VOCs and water. Each isotherm was obtained over the course of 2 h. The same scales are used in both parts of the figure to directly compare the response of the two SAMs. In (a), the equivalent coverage for the DIMP analyte at 50%-of-saturation is about 16 layers.

surface elemental analysis and by the replacement of the carbonyl band in the FTIR-ERS spectrum by carboxylate bands present at substantially lower energy.

Figure 2a presents nanogravimetric surface acoustic wave (SAW) data (frequency shift as a function of vapor-phase concentration) for six different organic analytes, as well as water, interacting with a MUA-Cu^{2+} SAM (Scheme 3).[18] The change in SAW-device frequency (Δf), due to the adsorption of vapor-phase molecules, is related to the mass loading per unit area (m_a) through the equation $\Delta f/f_o = -\kappa c_m f_o m_a$. Here, f_o is the SAW oscillation frequency (97 MHz), κ is the fraction of the distance between the centers of the transducers covered by the Au film (0.7), and c_m is the mass sensitivity coefficient of the device (1.33 $cm^2/(g\cdot MHz)$ for ST-cut quartz).[19−21]

The adsorption isotherms in Figure 2a indicate that multilayers form (based on molar volumes of the bulk liquids) on the surface at 50%-of-saturation vapor pressure ($p/p_{sat} = 0.5$) for all the analytes examined except iso-octane. The number of multilayers that adsorb gives a qualitative indication of the "range" of the monolayer/analyte interaction. It is thus interesting to note that the frequency shift for DIMP at 50% of saturation is consistent with the adsorption of approximately 16 layers of DIMP. This value is significantly larger than acetone, which has the next-highest equivalent molecular coverage (about eight monolayers). DIMP forms multilayers at the lowest partial pressure of the various analytes examined.

In contrast to the results for the MUA-Cu^{2+} surface, the same group of analytes interacting with a methyl-

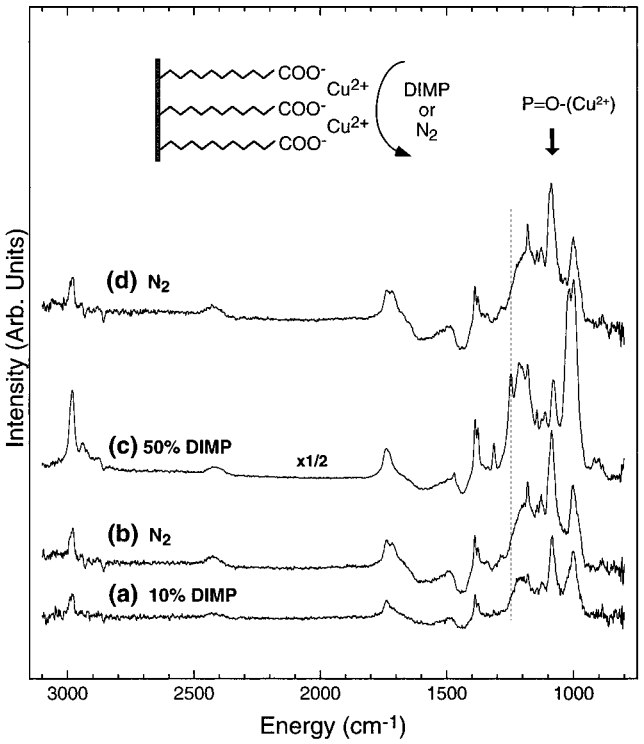

FIGURE 3. PM-FTIR spectra of a MUA-Cu^{2+} SAM during dosing with (a) 10%- and (c) 50%-of-saturation DIMP, and then (b and d) purging with N_2 for 30 min. The dashed line represents the phosphoryl band at 1214 cm^{-1} that is characteristic of liquid-phase DIMP. Note the change in scale for (c). Reprinted with permission from ref 23. Copyright 1997 Royal Society of Chemistry.

terminated SAM yield much lower adsorbed masses. As illustrated in Figure 2b, for example, there is no clear preference for the methyl-terminated surface by the organophosphonate (the same scales are used in both parts of Figure 2 to facilitate direct comparison of the two monolayer films). Nonspecific interactions between the analyte and the monolayer film (i.e., van der Waals forces) as well as specific interactions between adsorbing analyte molecules account for the relative differences in adsorbed mass. The point is that simple surface engineering gives rise to a distinct difference in chemical selectivity. Moreover, there is the unanticipated result that many monolayers of DIMP adsorb to the MUA-Cu^{2+} surface, which enhances both the dynamic range of the sensor and its sensitivity. We thought it would be useful to better understand this intriguing result.

Figure 3 shows polarization-modulation (PM)-FTIR difference spectra[22−25] of a MUA-Cu^{2+} SAM during dosing with 10%- and 50%-of-saturation DIMP (parts a and c, respectively) and after purging with N_2 for 30 min (parts b and d). This technique results in a spectrum only of DIMP interacting with the MUA-Cu^{2+} surface, and, therefore, DIMP present in the headspace of the flow cell is rendered transparent. The intense band at 1079 cm^{-1} (present in all the spectra) corresponds to the P═O stretching mode of DIMP. In liquid-phase DIMP this band occurs at 1245 cm^{-1}, but it is known that the phosphoryl oxygen of many phosphorus-containing compounds coordinate with metal ions to yield adducts characterized by a dramatic shift to lower energy.[26−29] Accordingly, we interpret the 1079 cm^{-1} band in terms of a very strong interaction between DIMP and Cu^{2+}. Interestingly, this band remains present even after purging with N_2 indicating that some of the DIMP remains irreversibly bound to the surface. However, the band at 1246 cm^{-1} (indicated by the dashed line in Figure 3), which is characteristic of liquid-phase DIMP, is only present during dosing at higher concentrations. On the basis of these results and a more detailed analysis of the spectra in Figure 3,[23] we conclude that the MUA-Cu^{2+} interface nucleates a solidlike phase of DIMP having a significantly lower vapor pressure than the liquid. A true liquidlike surface phase is only present at the highest DIMP concentrations. This lowering of the vapor pressure accounts for the very large number of monolayer equivalents of DIMP present on the surface at vapor pressures well below saturation. That is, although the outermost layers of DIMP are certainly too far from the SAM to "feel" its influence directly, the SAM provides a nucleation template whose effect is propagated through the nascent DIMP film.[23] This is a key result, because it implies that a single receptor (Cu^{2+} in this case) can bind many analyte molecules resulting in a significant degree of amplification compared to simple lock-and-key motifs.[30]

There are three important conclusions that arise from these DIMP dosing experiments. First, a synthetic step as simple as dipping a SAM into a metal-ion-containing solution yields a composite interface with significantly different chemical selectivity and sensitivity than either a methyl-terminated surface or the precursor acid. We have shown previously that the DIMP response is a strong function of the type of metal ion.[23] Second, the proper analytical tools, SAW devices and PM-FTIR spectroscopy in this case, yield real-time information that can be used to fully characterize the analyte/monolayer interaction chemistry. This is essential for optimizing and discovering new interfacial materials and processes. Third, although it is generally reasonable to assume that surface receptors have no significant effect beyond the adsorption of one or two monolayers of analyte, in the present case the effect of the surface chemical functionality extends to at least 16 adsorbed monolayer-equivalents of DIMP. As discussed in the next section, this result appears to be somewhat general.

Complex Bilayers

The metal-ion-terminated SAMs discussed in the previous section provide good class selectivity and sensitivity; however, it should be possible to gain additional control over selectivity by developing more complex bilayer structures. The prototype for this approach is calixarene (CA[*n*])-functionalized SAMs (Scheme 4). CA[*n*] belong to a class of "bucket-shaped" molecules consisting of *n* (= 4−11) phenyl subunits.[31] In the cone conformation,[31] CA[4] and CA[6] have inner cavity diameters of 6.3 and 7.9 Å, and outer upper-rim diameters of 13.6 and 18.0 Å, respectively.[32] The host−guest interactions associated

Scheme 4

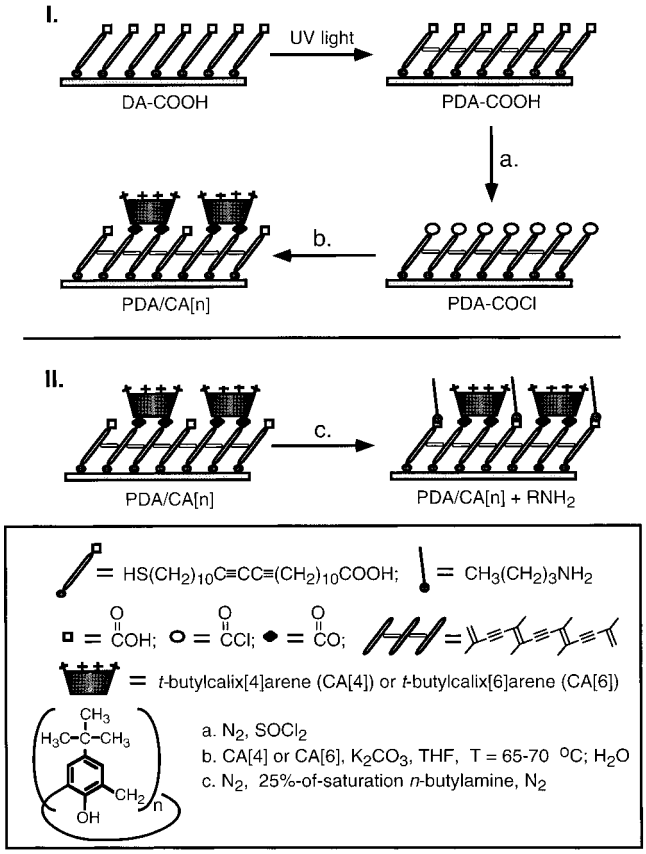

with the hydrophobic CA[4] and CA[6] cavities are usually weak, since they involve principally van der Waals, induced-dipole, and π-stacking interactions. A resilient intermediate attachment layer based on photopolymerized diacetylenic SAMs, rather than the simple *n*-alkanethiols described in the previous sections, was used for this study to enhance bilayer stability (Scheme 4).[33] In this section, we discuss the linking chemistry that leads to calixarene immobilization and examine the role the calixarene cavities play in recognizing three volatile organic compounds (VOCs) using SAW device-based gravimetry.

Part I of Scheme 4 illustrates the synthesis of the polydiactylene/calixarene (PDA/CA[*n*]) bilayers.[11] Monolayers were prepared by soaking a Au substrate in a solution of the acid-terminated diacetylene, and then polymerizing with UV light.[34] Following polymerization, the substrates were exposed to $SOCl_2$ vapor to convert the carboxylic acid functional groups to the more reactive acid chloride (PDA-COCl). The hydroxyl groups on the lower rims of CA[4] and CA[6] react with PDA-COCl to yield an ester linkage.

Part II of Scheme 4 illustrates the irreversible adsorption of vapor-phase *n*-butylamine onto the CA[*n*] bilayer-coated SAW devices. This strategy is used as an indirect nanogravimetric titration method to estimate the fractional surface coverage of CA[*n*] on the PDA surface. By measuring the difference in *n*-butylamine mass loading on the PDA-COOH and PDA/CA[*n*] surfaces, we calculate that CA[4] and CA[6] cover 58 and 61%, respectively, of the PDA-COOH surface.[11] The irreversibly bound *n*-butylamine serves a secondary purpose by effectively filling voids between calixarenes, thereby hindering VOC access to these domains.

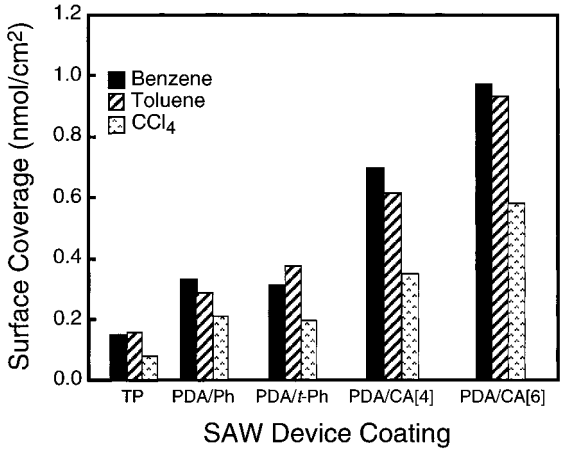

FIGURE 4. Comparison of the average surface coverage for TP-, PDA/Ph-, PDA/*t*-Ph-, PDA/CA[4]-, and PDA/CA[6]-coated SAW devices exposed to benzene, toluene, and CCl_4 present at 25% of saturation in dry N_2. The data shown were obtained prior to *n*-butylamine dosing (part II of Scheme 4), but VOC surface coverages within 5% of these values were measured after amine adsorption onto the acid groups remaining after CA[*n*] functionalization. This result suggests that the voids between CA[*n*]s play an insignificant role in the overall interfacial response of this surface.

Figure 4 shows a summary of the average mass-loading data obtained by dosing thiophenol (TP)-, phenyl-terminated PDA (PDA/Ph)-, 4-*tert*-butylphenyl-terminated PDA (PDA/*t*-Ph)-, PDA/CA[4]-, and PDA/CA[6]-coated SAW devices with 25%-of-saturation benzene, toluene, and CCl_4. The TP, PDA/Ph, and PDA/*t*-Ph control surfaces were chosen because of their chemical similarity to the upper rim of the PDA/CA[*n*] bilayers, but note the absence of a structurally distinct cavity on the control surfaces. TP is bound to the Au substrate directly through a thiolate interaction while Ph and *t*-Ph are linked to the PDA layer through ester linkages in the same manner as CA[*n*].

We dosed the TP, PDA/Ph, and PDA/*t*-Ph surfaces to determine whether VOC adsorption is enhanced at the CA[*n*] surfaces on the basis of specific interactions with discrete CA[*n*] macrocycles or whether nonspecific interactions, promoted by the calixarene *tert*-butylphenyl groups, dominate adsorption. Referring to Figure 4, the magnitude of VOC adsorption is much smaller, typically less than 50%, for the three control surfaces compared to the PDA/CA[*n*] bilayers. We might expect that if adsorption on the CA[*n*] surfaces results primarily from nonspecific interactions, then a similar extent of VOC adsorption would occur at these control surfaces.

On the basis of the data in Figure 4, we conclude that the calixarene cavities figure prominently in the chemical selectivity of these interfaces. Evidence for this comes from the significantly enhanced surface coverage of benzene and toluene on the CA[*n*] surfaces compared to TP, PDA/Ph, and PDA/*t*-Ph surfaces. The CA[4] and CA[6] cavities have interior diameters of 6.3 and 7.9 Å, respectively. The benzene and toluene molecules have

Scheme 5

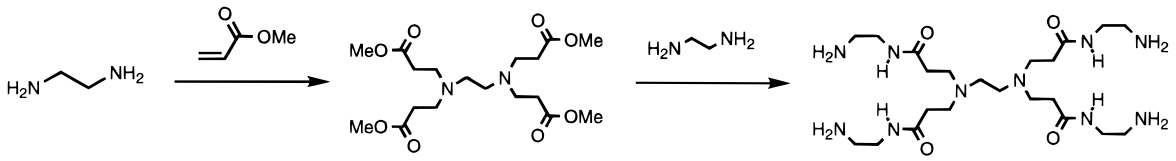

estimated molecular diameters, across the 2,6 hydrogens, of 6.3 Å (CPK models), and their flat, discus-like shapes are conducive to π-stacking within the CA[*n*] cavities. Thus, we conclude that enhanced selectivity for benzene and toluene results from a favorable specific interaction between the hydrophobic cavities of the two calixarenes and the aromatic compounds. Additional evidence for analyte inclusion into the calixarenes comes from a comparison of the CCl_4 data. The PDA/CA[6] bilayer is significantly more receptive to the CCl_4 probe than any of the other surfaces. We interpret this result in terms of size and shape selectivity. Unlike benzene or toluene, CCl_4 has spherical symmetry and is too large (approximately 6.4 Å in diameter based on CPK models) to fit entirely within the CA[4] cavity, but can be accommodated by CA[6].

Dosing the bilayer-coated SAW devices with VOCs before and after exposure to *n*-butylamine allows us to better understand the role of the calixarene cavities relative to nonspecific adsorption at, for example, defect sites between CA[*n*] molecules. Frequency shifts associated with analyte dosing of the CA[4]- and CA[6]-coated devices before and after irreversible adsorption of *n*-butylamine are within 5% of a monolayer for all three VOCs. This strongly suggests that enhanced VOC adsorption at the calixarene-modified surface results from the cavities rather than interstitial voids.

There is one final very interesting issue raised by the data in Figure 4. As discussed earlier, CA[4] and CA[6] have estimated surface coverages of 58 and 61%, respectively, which corresponds to 0.06 and 0.04 nmol/cm^2, respectively. Dosing the CA[4] and CA[6] surfaces with 25%-of-saturation benzene yields mass loadings of 0.70 and 0.97 nmol/cm^2, respectively. Since a 1:1 host/guest stoichiometry would yield maximum benzene coverages equal to the CA[4] and CA[6] surface concentrations, we conclude that the calixarenes act as templates that nucleate benzene into clusters that average 10−20 molecules each and permit it (as well as some of the other probe molecules) to adopt surface conformations that are to some degree solidlike. That is, the phase of the surface-confined benzene must have a lower vapor pressure than liquid benzene; otherwise, it would immediately desorb at the partial benzene pressure used for these experiments. Importantly, on the three noncalixarene surfaces shown in Figure 4, the surface concentration of benzene does not exceed half of the maximum single-monolayer coverage (roughly the same as the PDA monolayer, 0.94 nmol/cm^2, after accounting for surface roughness), which provides an important control that strongly suggests the fully reproducible data for CA[4] and CA[6] surfaces are correct. Note that this is precisely the same type of nucleation effect observed for the MUA-Cu^{2+} bilayers described in the previous section, suggesting that this phenomenon might be sufficiently general to be very useful for chemical sensor applications.

Dendrimers

Dendrimers are polymers prepared by repetitive branching from a central core.[35] Dendrimer structure is best illustrated by the synthetic steps required to prepare the zeroth generation (G0) of commercially available poly(amidoamine) (PAMAM) Starburst dendrimers (Scheme 5),[36] which are based on an ethylenediamine core, amidoamine repetitive branch units, and primary amine terminal groups. A dendrimer's size increases with generation number and its molecular conformation evolves. G0 and G1 dendrimers have an expanded or "open" configuration, but as the size increases, crowding of the surface functional groups causes dendrimers to adopt a spherical or globular structure.

As illustrated by the dendrimer branch shown in Scheme 6, these materials have several attractive attributes for sensing applications. First, they are dense on the outside but somewhat hollow on the inside. This means that VOCs can sorb into the interior of the dendrimer and be size selected by synthetically controlling the dimensions of the openings that result from packing of the outermost branches. Second, the chemical identity of both the exterior and interior of the dendrimer can be tailored for specific applications, which greatly enhances molecular specificity. Finally, dendrimers are three-dimensional objects, so they are inherently more highly functionalized than the *n*-alkanethiol SAMs or SAM-based bilayers described previously. This leads to increased sensitivity and synthetic flexibility.

We have used three different methods for preparing surface-confined dendrimer monolayers. As shown in part a of Scheme 7, dendrimers can be anchored to surfaces via a single-component, intermediate SAM attachment layer.[12] For example, activation of the terminal groups of a MUA SAM followed by exposure to amine-terminated PAMAM dendrimers leads to covalent attachment via amide linkages. Following immobilization, the remaining amine groups can be functionalized with exoreceptors of various types. Spectroscopic analysis indicates that this surface-attachment protocol results in a significant flattening of the dendrimer as shown in the illustration; this structural distortion affects the average opening size and endoreceptivity of these materials.

It is possible to reduce the magnitude of confinement-induced morphological changes by using a mixed-SAM attachment layer consisting of a low surface concentration

Scheme 6

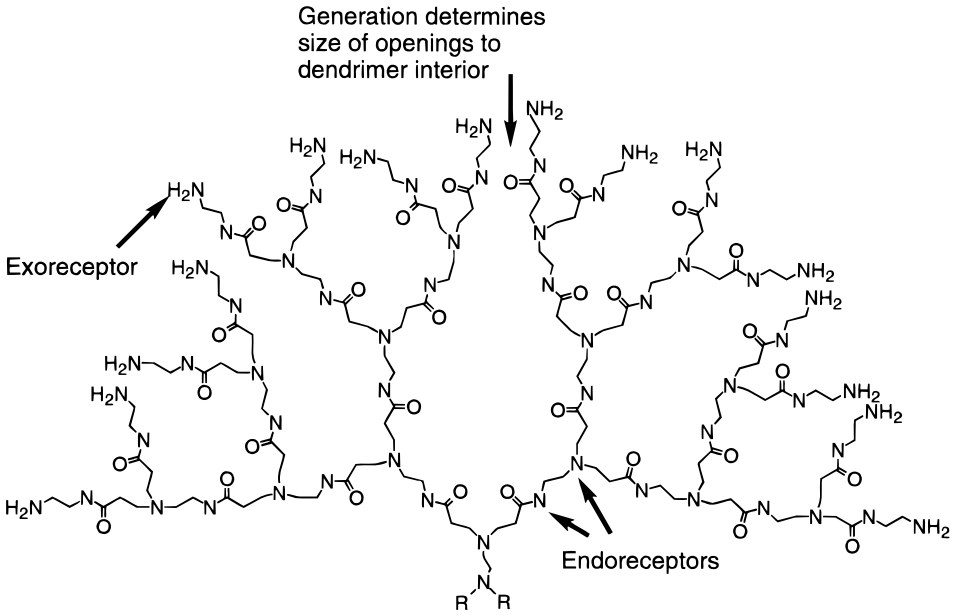

of an *n*-alkanethiol terminated in a reactive group, such as MUA, diluted by a much shorter, unreactive methyl-terminated *n*-alkanethiol (part b of Scheme 7).[37] Activation of the small percentage of acid groups results in linking of one or just a few terminal groups of each dendrimer to the surface. Distortion is avoided because the remaining terminal amine groups neither react with nor wet the dominant methyl-terminated component of the SAM. Using this approach, we have shown that the surface immobilization is possible either before or after exoreceptor functionalization of the dendrimer terminal groups.

Dendrimers can also be immobilized directly on Au without the need for intermediate attachment layers (part c of Scheme 7).[38,39] This is a consequence of a strong aggregate interaction between the many primary amine terminal groups per dendrimer and the Au surface. Thus, simply soaking a Au substrate in a dilute solution of a G4 PAMAM dendrimer results in nearly full monolayer coverage. Such monolayers are not as stable as those prepared by covalent linking, but their resilience can be enhanced by subsequent adsorption of a partial *n*-alkanethiol monolayer. This action results in compression of the dendrimer by the *n*-alkanethiol (part c of Scheme 7) and formation of a hydrophobic pocket that protects the amine/Au interactions.

Finally, we have also demonstrated two methods for increasing the number density of dendrimers on the surface. First, dendrimers can be attached to high-surface-area Au colloids using any of the attachment protocols described above.[40] Second, dendrimer-containing nanocomposite polymer films can be prepared on planar substrates using a very simple synthetic approach.[41]

Scheme 7

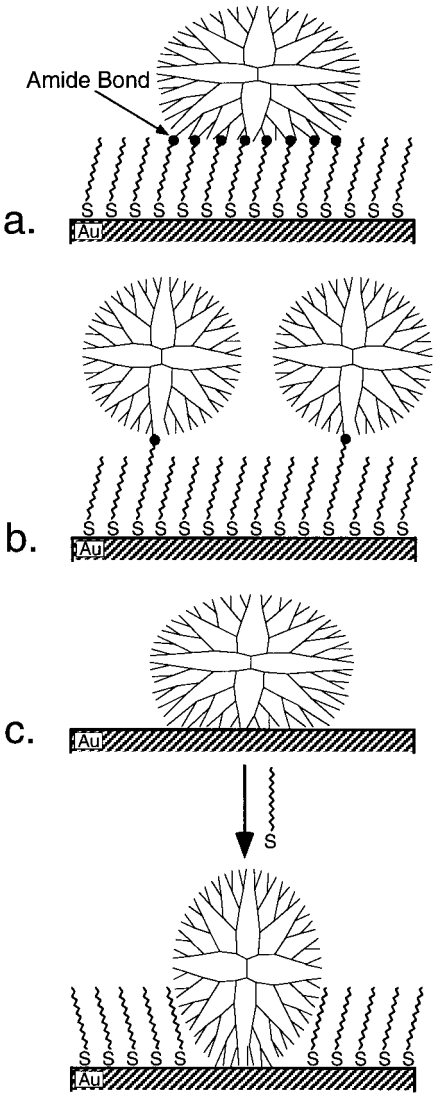

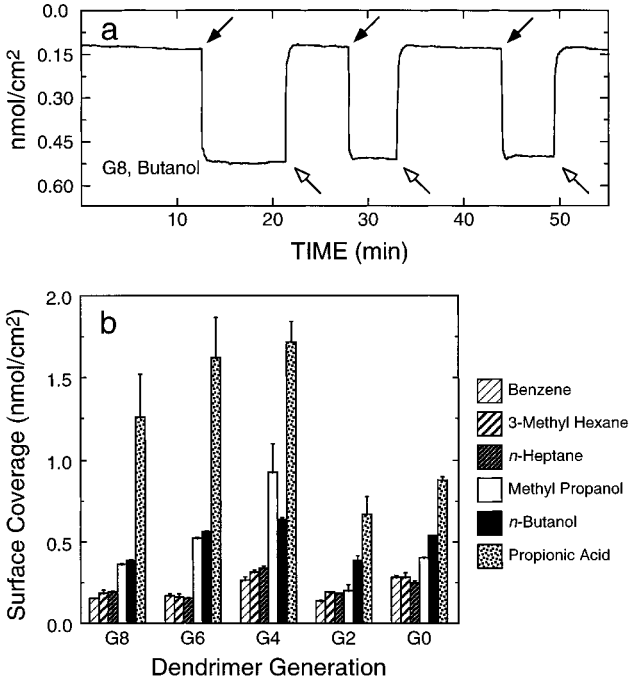

FIGURE 5. (a) Unprocessed response from a G8 PAMAM dendrimer-modified SAW device dosed with vapor-phase butanol. (b) Results from dosing dendrimer-modified SAW devices with six VOCs. Error bars represent the standard deviation of the average results from three devices, each cycled three times per dosant.

This strategy is especially powerful since it is based on layer-by-layer growth, which permits excellent control over film thickness. The important point is that, regardless of the surface-immobilization strategy used, dendrimers have tremendous potential as interfacial materials for chemical sensing because of their morphological characteristics, high degree of synthetic flexibility, and multiple reactive sites per dendrimer.

To illustrate the suitability of dendrimer surfaces as chemically sensitive interfaces and demonstrate some of the principles that govern their performance, we modified SAW devices with dendrimers as shown in part a of Scheme 7 and dosed them sequentially with VOCs having different functional groups (Figure 5).[12] Figure 5a is an example of unprocessed data from a typical SAW experiment. It illustrates how the G8 dendrimer-modified device response to butanol possesses three of the essential attributes of an ideal chemical sensor: the response to dosants is very rapid with no detectable permeation transient, the signal-to-noise ratio is excellent, and the response is fully reversible.

Figure 5b summarizes the results of many dosing experiments such as those shown in Figure 5a. The mass-loading response of the three different classes of analytes decreases in the order acid > alcohols > alkanes and aromatics. This response order is more pronounced for the G4−G8-modified surfaces and is dictated by the PAMAM structure, which possesses hydrogen-bonding exo- and endoreceptors (Scheme 6). The G4-modified surface is the most responsive material because, although it is the smallest of the spheroidal dendrimers, its interior endoreceptors are most accessible because of enhanced permeability compared to the denser G6 and G8 dendrimer surfaces. G0 and G2 dendrimer films are not as effective at discriminating between the three different classes of analytes since these surfaces have few or no free amine terminal groups and no coherent endoreceptive ability. The important point is that the chemical and structural characteristics of the dendrimers can be used to predict the classes of analytes they are likely to interact with. Additionally, the extent of dendrimer penetration by the analyte is governed by its size in a very intuitive way.

Summary and Conclusions

Array-based chemical sensors are likely to play an increasing role in future analytical detection systems. The heart of these devices are the chemically sensitive materials affixed to their transducers, and chemists clearly have an expanding role to play in designing, characterizing, and testing these materials. Superior interfacial materials must be synthetically versatile so that classes of materials, like the SAMs and dendrimers described in this Account, can be easily and inexpensively manipulated to yield families of materials that provide chemically independent responses in the presence of target analytes. Additionally, attachment of the materials to suitable transducers must be straightforward. It is also advantageous to be able to predict the sensor response based on simple chemical principles and a knowledge of the structural and chemical properties of the interfacial materials and analytes. For example, we predicted that the MUA-Cu^{2+} surface would preferentially bind DIMP because Cu^{2+} is a hydrolysis catalyst for organophosphorus compounds. It also follows from chemical intuition that the responses of the PAMAM dendrimer interfaces to VOCs should follow the profile shown in Figure 5. Finally, the time response and sensitivity of the interfacial materials must be considered. SAMs generally provide very fast responses, but their sensitivity and dynamic range is restricted by the limited number of receptors inherent to a planar surface. Note, however, that our discovery that SAM receptors can bind analytes in a much-greater-than-1:1 stoichiometry provides some relief to this limitation.[18,23] Thicker materials such as polymers provide a much larger number of receptors, and thus enhance sensitivity compared to monolayers, but permeation transients may render them inappropriate for time-sensitive applications such as chemical-agent detection or high-throughput applications such as those associated with airport security screening. Perhaps quasi-three-dimensional materials such as the dendrimer monolayers or monolayers affixed to high-surface-area substrates[42] will help to provide a compromise between rapid response and low limits of detection in future-generation devices.

We acknowledge the hard work and intellectual contributions of our research group members past and present: Merlin L. Bruening, Daniel L. Dermody, Maurie E. Garcia, Larry J. Kepley, Taisun Kim, Laurel J. McEllistrem, Robert Peez, Alan W. Staton, Li Sun, Ross C. Thomas, Hideo Tokuhisa, Mona Wells, Chuanjing

Xu, and Huey Yang. The authors also gratefully acknowledge Mark Kaiser of Dendritech, Inc. (Midland, MI) for supplying samples of the Starburst PAMAM dendrimers used in this work. We also thank Professor Robert M. Corn for invaluable assistance in setting up the PM-FTIR experiment. Finally, the work at Texas A&M would not have been possible without generous and sustained financial support from the National Science Foundation (CHE-9313441), the Office of Naval Research, the Robert A. Welch Foundation, and Sandia National Laboratories. Work at Sandia was supported by the U.S. Department of Energy under Contract DE-AC04-94AL85000. Sandia is a multiprogram laboratory operated by Sandia Corporation, a Lockheed-Martin Company, for the U.S. Department of Energy.

References

(1) Ricco, A. J.; Crooks, R. M.; Osbourn, G. C. *Acc. Chem. Res.* **1998**, *31*, 289.
(2) Osbourn, G. C.; Bartholomew, J. W.; Ricco, A. J.; Frye, G. C. *Acc. Chem. Res.* **1998**, *31*, 297.
(3) Swalen, J. D.; Allara, D. L.; Andrage, J. D.; Chandross, E. A.; Garoff, S.; Israelachvili, J.; McCarthy, T. J.; Murray, R.; Pease, R. F.; Rabolt, J. F.; Wynne, K. J.; Yu, H. *Langmuir* **1987**, *3*, 932.
(4) Ulman, A. *An Introduction to Ultrathin Organic Films From Langmuir−Blodgett to Self-Assembly*; Academic: San Diego, 1991.
(5) Dubois, L. H.; Nuzzo, R. G. *Annu. Rev. Phys. Chem.* **1992**, *43*, 437.
(6) Nuzzo, R.; Allara, D. L. *J. Am. Chem. Soc.* **1983**, *105*, 4481.
(7) Bain, C. D.; Troughton, E. B.; Tao, Y.-T.; Evall, J.; Whitesides, G. M.; Nuzzo, R. G *J. Am. Chem. Soc.* **1989**, *111*, 321.
(8) Chailapakul, O.; Sun, L.; Xu, C.; Crooks, R. M. *J. Am. Chem. Soc.* **1993**, *115*, 12459.
(9) Chidsey, C. E. D.; Loiacono, D. N. *Langmuir* **1990**, *6*, 682.
(10) Nuzzo, R.; Zegarski, B. R.; Dubois, L. H. *J. Am. Chem. Soc.* **1987**, *109*, 733.
(11) Dermody, D. L.; Crooks, R. M.; Kim, T. *J. Am. Chem. Soc.* **1996**, *118*, 11912.
(12) Wells, M.; Crooks, R. M. *J. Am. Chem. Soc.* **1996**, *118*, 3988.
(13) Zhou, Y.; Bruening, M. L.; Bergbreiter, D. E.; Crooks, R. M.; Wells, M. *J. Am. Chem. Soc.* **1996**, *118*, 3773.
(14) Duevel, R. V.; Corn, R. M. *Anal. Chem.* **1992**, *64*, 337.
(15) Sun, L.; Kepley, L. J.; Crooks, R. M. *Langmuir* **1992**, *8*, 2101.
(16) Sun, L.; Crooks, R. M.; Ricco, A. J. *Langmuir* **1993**, *9*, 1775.
(17) Wagner-Jauregg, T.; Hackley, B. E., Jr.; Lies, T. A.; Owens, O. O.; Proper, R. *J. Am. Chem. Soc.* **1955**, *77*, 922.
(18) Thomas, R. C.; Yang, H. C.; DiRubio, C. R.; Ricco, A. J.; Crooks, R. M. *Langmuir* **1996**, *12*, 2239.
(19) Ricco, A. J.; Frye, G. C.; Martin, S. J. *Langmuir* **1989**, *5*, 273.
(20) Hughes, R. C.; Ricco, A. J.; Butler, M. A.; Martin, S. J. *Science* **1991**, *254*, 74.
(21) Ricco, A. J. *Electrochem. Soc. Interface* **1994**, *3*, 38.
(22) Barner, B. J.; Green, M. J.; Sáez, E. I.; Corn, R. M. *Anal. Chem.* **1991**,*63*, 55.
(23) Crooks, R. M.; Yang, H. C.; McEllistrem, L. J.; Thomas, R. C.; Ricco, A. J. *Faraday Discuss.* **1997**, *107*, 285.
(24) Porter, M. D. *Anal. Chem.* **1988**, *60*, 1143A.
(25) Xu, C.; Sun, L.; Kepley, L. J.; Crooks, R. M.; Ricco, A. J. *Anal. Chem.* **1993**, *65*, 2102.
(26) Guilbault, G. G.; Scheide, E. P. *J. Inorg. Nucl. Chem.* **1970**, *32*, 2959.
(27) Karayannis, N. M.; Pytlewski, L. L.; Owens, C. *J. Inorg. Nucl. Chem.* **1980**, *42*, 675.
(28) Guilbault, G. G.; Das, J. *J. Phys. Chem.* **1969**, *73*, 2243.
(29) Goodgame, D. M. L.; Cotton, F. A. *J. Chem. Soc.* **1961**, *3735* and references therein.
(30) There is a possible alternative explanation for DIMP multilayer formation brought to our attention at a recent Faraday Discussion (see ref 23). Cu^{2+} could reversibly "dissolve"into the DIMP adlayer resulting in a highly concentrated salt solution, which in turn could lead to boiling-point elevation (i.e., vapor pressure lowering). At present we cannot rule out this plausible alternative mechanism.
(31) Gutsche, C. D. *Calixarenes*; The Royal Society of Chemistry: London, 1989.
(32) The edge-to-edge internal cavity diameters and the upper outer-rim diameters of CA[4] and CA[6], in the cone conformation, were estimated from CPK models.
(33) Kim, T.; Chan, K. C.; Crooks, R. M. *J. Am. Chem. Soc.* **1997**, *119*, 189.
(34) Kim, T.; Chan, K. C.; Crooks, R. M.; Ye, Q.; Sun, L. *Langmuir* **1996**, *12*, 6065.
(35) Zeng, F.; Zimmerman, S. C. *Chem. Rev.* **1997**, *97*, 1681−1712.
(36) "Starburst" is a trademark owned by Dendritech, Inc. (Midland, MI).
(37) Tokuhisa, H.; Crooks, R. M. *Langmuir*, **1997**, *13*, 5608.
(38) Zhao, M.; Tokuhisa, H.; Crooks, R. M. *Angew. Chem., Int. Ed. Engl.* **1997**, *13*, 5608.
(39) Tokuhisa, H.; Zhao, M.; Baker, L. A.; Phan. V. T.; Dermody, D. L.; Garcia, M. E.; Peez, R.; Crooks, R. M. *J. Am. Chem. Soc.*, in press.
(40) Garcia, M.; Baker, L.; Crooks, R. M. *Abstracts of Papers*, 215th National Meeting of the American Chemical Society, Dallas, TX; American Chemical Society: Washington, DC, 1997; COLL 198.
(41) Liu, Y.; Bruening, M. L.; Bergbreiter, D. E.; Crooks, R. M. *Angew. Chem., Int. Ed. Engl.* **1997**, *36*, 2114.
(42) Ricco, A. J., Sandia National Laboratories. Personal communication, 1997.

AR970246H